Journal of Applied Fluid Mechanics, Vol. 11, No. 1, pp. 191-204, 2018.
Available online at www.jafmonline.net, ISSN 1735-3572, EISSN 1735-3645.
DOI: 10.29252/jafm.11.01.27935

Characterization of Vortex Development and Thermo-Solutal Transfers on Confined Wall Jets Submitted to Suction or Blowing: Part 2

S. Mejri[1†] and M. A. Knani[12]

[1]*LMF : Laboratoire de Mécanique des Fluides-Département de Physique, Faculté des Sciences de Tunis, Université de Tunis-Elmanar, 1000 Tunis, Tunisie.*
[2] *Institut Préparatoire aux Etudes d'Ingénieurs de Tunis., Université de Tunis, 2 rue Nehru, 1080 Montfleury,Tunisie.*

†*Corresponding Author Email: mejrisa3ida@gmail.com*

(Received May 1, 2017; accepted August 23, 2017)

ABSTRACT

A computational study is conducted to explore the effect of vertical wall suction or blowing on two-dimensional confined wall jet hydrodynamic characteristics. Using an implicit finite volume technique in Cartesian coordinate system, several parameters have been investigated for a wide range of Lewis numbers by fixing the Prandtl number at 7 that corresponds to water. The main purpose is to analyze the control size and location effectiveness on the flow pattern as well as heat and mass transfer rates. Detailed numerical simulations demonstrated that as the local blowing is moved downstream, discrete vortex formation begins at a critical location then shedding phenomenon occurs behind the slot at advanced positions. Since the flow dynamic structure is mainly altered, averages skin friction and thermo-solutal coefficients distributions are largely influenced. Approximately for $x_s \leq 4$ (upstream of the natural vortex emission position), Nusselt and Sherwood numbers slightly increase with the control location x_s. However, they gradually decrease as the blowing slot approaches the domain exit. Optimum values were obtained when locating the slot just downstream of the uncontrolled Kelvin-Helmholtz instability onset. Furthermore, computations illustrated that an appropriate suction slot length selection could be a simple and efficient tool to delay or even suppress natural structure emission and development. This choice is essentially related to the recirculation cell size.

Keywords: Confined wall jet; Flow control; Blowing slot position; Suction slot length; Lewis number.

NOMENCLATURE

A	aspect ratio
C^*	dimensional concentration
C	dimensionless concentration
C_0^*	dimensional ambiant concentration
C_0	dimensionless ambient concnetration
$\overline{C_f}$	average skin friction coefficient Eq. (11)
$C_f(x)$	local skin friction coefficient
C_w^*	dimensional concentration at the wall
C_w	dimensionless concentration at the wall
ΔC^*	concentration difference between the wall and the ambiant fluid
D	studied domain width
D_{Mass}	mass diffusivity
g	acceleration of the gravity
H	inlet nozzle width
k	thermal conductivity of the fluid
L	studied domain length
Le	Lewis number
l_{Rc}	recirculation cell core length
l_s	suction or blowing slot length
N	buoyancy ratio
$\overline{Nu}$	average Nusselt number Eq.(9)
$Nu(x)$	local Nusselt number
p^*	pressure
p	dimensionless pressure
Pr	Prandtl number
Re	Reynolds number
Sc	Schmidt number
$\overline{Sh}$	average Sherwood number Eq. (10)
$Sh(x)$	local Sherwood number
T^*	dimensional temperature
T	dimensionless temperature
T_0^*	dimensional ambient temperature
T_0	dimensionless ambient temperature
T_w^*	dimensional temperature at the wall
T_w	dimensionless temperature at the wall
ΔT^*	temperature difference between the wall and the ambiant fluid
t^*	dimensional time
t	dimensionless time

U_0	free stream velocity
(u, v)	velocity components in x, y directions
v_w	suction or blowing velocity
(x^*, y^*)	dimensional Cartesian coordinates
(x, y)	dimensionless Cartesian coordinates
x_s	suction or blowing slot position
α	thermal diffusivity
β_T	coefficient of thermal expansion
β_c	coefficient of solutal expansion
Δ	difference value
δ	wall jet width
$\delta_{1/2}$	wall jet half-width
ϑ	kinematic viscosity
ρ^*	fluid density
ρ	dimensionless fluid density

1. INTRODUCTION

Laminar fluid flow past an unconfined or confined wall jet represents a basic problem of fundamental importance due to its numerous practical engineering applications like aerodynamics, vehicle construction and electronics cooling. In order to enhance the performance of these geometries, various control techniques have been elaborated. Among such methods, suction or blowing is one of the most promising and the highest growing process due to its widespread accessibility. An extensive number of studies have then been conducted, tending to improve the comprehension and effectiveness of such active means. Several approaches can be performed such as steady (Chen *et al.* 2006; Radespiel *et al.* 2016) or pulsed (Marom *et al.* 2015; Marom *et al.* 2016) fluid amounts imposed from one or multiple slots (Sun and Hamdani 2001; Zhao *et al.* 2015) either tangentially or perpendicularly (Yousefi *et al.* 2013). Kim and Sung (2003) performed direct numerical simulations of a spatially evolving turbulent boundary layer. By comparing the flow behavior of the system maintained under steady conditions with that in the occurrence of periodic blowing, they showed that this last one causes the enhancement of turbulence energy intensities near the wall. Wilson *et al.* (2013) conducted a flow-control study using steady suction and pulsed blowing on an axisymmetric bluff body. Results showed that suction alone has a restricted ability to delay separation and reduce drag on this geometry. An optimal single row suction location of 0.04 upstream of the mean separation position was determined for the considered Reynolds number range. Moreover, farther upstream locations were found to be less effective, whereas farther downstream ones become detrimental. In the other hand, authors showed that addition of pulsed blowing allows separation delay to the trailing edge to be nullified. In terms of drag reduction, it was demonstrated that oscillatory blowing without suction was more beneficial than one row of suction holes but less than distributed suction. Sohankar *et al.* (2015) investigated the effects of uniform suction and blowing positioned on three different surfaces of a square cylinder in order to attain optimum configuration. Zhang *et al.* (2016) conducted a numerical simulation to study the laminar flow past a square cylinder confined in a channel subjected to a locally uniform blowing or suction speed positioned at the top and bottom channel walls. The numerical results showed that wall blowing has a stabilizing influence on the flow accordingly the corresponding critical Reynolds number rises monotonically with the blowing velocity. When increasing or decreasing Reynolds number continuously at a fixed suction speed, hysteretic phenomena of mode exchanges were observed.

The interaction of suction and pulsed blowing with a laminar boundary layer was analyzed by Seifert and Marom (2015). Conducted simulations demonstrated that while oscillatory blowing has a strong effect on the flow evolution, the steady suction introduced upstream has a crucial role on the AFC (active flow control) system efficiency. Sattarzadeh and Fransson (2017) used discrete suction deployed in a flat plate boundary layer to generate spanwise mean velocity gradients in order to delay laminar to turbulent transition onset.

Actuality, exploring all potential models and interfering factors (imposed velocity ratio and direction; slots number, length and position…) requires an extremely large number of flow simulations. In general, a few major parameters are varied in a series of numerical computations with the goal of finding an optimal configuration. Earlier numerical study of double diffusive natural convection in a vertical porous enclosure conducted by Zhao *et al.* (2007) showed that the Lewis number has a direct bearing on heat and mass transfer coefficients. As thermal Darcy–Rayleigh number increases, the segment location allowing maximum thermo-solutal transfer rates moves from the center toward the bottom of the enclosure. Trompoukis *et al.* (2008) presented a step-by-step optimization study, to maximize the reduction in viscous flow losses, in which the slot location and geometry as well as the blowing or suction characteristics were sequentially selected. Chen *et al.* (2010) discussed the relative effectiveness of blowing and suction in controlling separation and circulation. They demonstrated the existence of a threshold momentum input where blowing becomes more effective than suction. Later, Yousefi *et al.* (2013) focused on tangential and perpendicular blowing and suction slot geometry optimization including jet width and amplitude effects. Chen *et al.* (2015) analyzed the control effectiveness on aerodynamic forces and alternate vortex shedding suppression as a function of suction holes azimuthal position, spanwise spacing and flow rate.

As mentioned above, blowing or suction has been widely employed as an efficient method for controlling wall bounded flows. In the present work, we aim to find out the suitable control conditions to minimize or enhance thermo-solutal transfer and

pressure forces within confined wall jet flow. Therefore, some key parameters are discussed in wide ranges namely the Lewis number as well as suction slot position and length. A particular intention is given to clarify vortices development and shedding mechanism inhibition effects.

2. FLOW CONFIGURATION AND NUMERICAL TOOLS

The computational domain and the Cartesian coordinates system are represented in Fig. 1. The geometry extent is chosen so that the flow can be considered as two-dimensional. Studied dimensions are $L \times D \times H = 10 \times 1 \times 0.25$. Here L, D and H represent the domain length, width and the nozzle high, respectively.

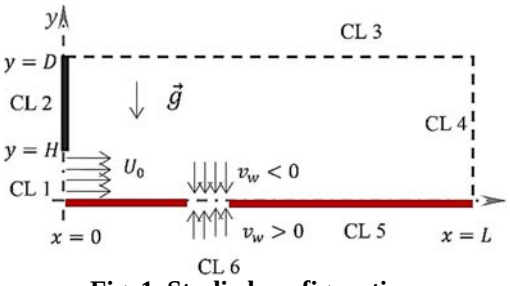

Fig. 1. Studied configuration.

The considered fluid is water ($Pr = 7$) issuing from a rectangle nozzle into an infinite domain filled with the same fluid at the concentration $C = C_0$. The suction or blowing slot is placed on the bottom wall maintained at a different temperature ($T_w = 1$). It is worth mentioning that suction corresponds to $v_w < 0$, blowing to $v_w > 0$ and $v_w = 0$ to impermeable wall.

The chosen boundary conditions are illustrated in Table 1. At the domain inlet, a uniform profile ($U_0 = 1$) is deployed for velocity. Convective boundary conditions along with zero second-order partial derivative of the *U* velocity ($\partial^2 U/\partial x^2 = 0$)

are set at the jet exit and no-slip conditions are prescribed at the flat walls ($U = V = 0$). Note that concentrated water ($C_w = 1$) is introduced either from the blowing slot or the jet entry in suction case. This configuration seems to provide the best alternative to assess the control effectiveness on the present problem.

Four velocities were initially tested: $v_w = \pm 0.2$ and $v_w = \pm 0.5$. For the highest values, vortex shedding was suppressed. However, when the imposed velocity was set equal to $|v_w| = 0.2$ (which is about 20% of the streamwise mean velocity), this phenomena persists which is effectively required here to evaluate the studied parameters effects on altering the flow structure.

With reference to Newtonian incompressible fluid of constant physical properties, the governing equations are written in dimensionless form in Cartesian coordinates system as:

The Boussinesq approximation :

$$\rho = \rho_0[\,1 - \beta_T(T - T_0) - \beta_C(C - C_0)] \quad (1)$$

Continuity Equation :

$$\nabla.\vec{V} = 0 \quad (2)$$

Momentum Equations :

$$\frac{\partial \vec{V}}{\partial t} + (\vec{V}.\nabla)\vec{V} = -\nabla p + \frac{1}{Re}\Delta\vec{V} - \left[\left(\frac{Gr_T}{Re^2}\right)T + \left(\frac{Gr_S}{Re^2}\right)C\right]\vec{K} \quad (3)$$

Heat Equation :

$$\frac{\partial T}{\partial t} + \vec{V}.\nabla T = \frac{1}{Pr \times Re}\Delta T \quad (4)$$

Solutal diffusion Equation :

$$\frac{\partial C}{\partial t} + \vec{V}.\nabla C = \frac{1}{Sc \times Re}\Delta C \quad (5)$$

Table 1 Boundary conditions

Blowing	
CL1	$U_0 = 1\,;\, V = 0\,;\, \frac{\partial T}{\partial x} = 0$ and $C = C_0$
CL2	$U = 0\,;\, V = 0\,;\, \frac{\partial T}{\partial x} = 0$ and $\frac{\partial C}{\partial x} = 0$
CL3	$\frac{\partial U}{\partial y} = 0\;;\, V = 0\,;\, T = 0$ and $\frac{\partial C}{\partial y} = 0$
CL4	$\frac{\partial^2 U}{\partial x^2} = 0\;;\, \frac{\partial V}{\partial x} = 0\,;\, \frac{\partial T}{\partial x} = 0$ and $\frac{\partial C}{\partial x} = 0$
CL5	$U = 0\,;\, V = 0\,;\, T_w = 1$ and $\frac{\partial C}{\partial y} = 0$
CL6	$U = 0\,;\, V = V_0\,;\, T = T_0$ and $C_w = 1$
Suction	
CL1	$U_0 = 1\,;\, V = 0\,;\, \frac{\partial T}{\partial x} = 0$ and $C = 1$
CL2	$U = 0\,;\, V = 0\,;\, \frac{\partial T}{\partial x} = 0$ and $\frac{\partial C}{\partial x} = 0$
CL3	$\frac{\partial U}{\partial y} = 0\;;\, V = 0\,;\, T = 0$ and $\frac{\partial C}{\partial y} = 0$
CL4	$\frac{\partial^2 U}{\partial x^2} = 0\;;\, \frac{\partial V}{\partial x} = 0\,;\, \frac{\partial T}{\partial x} = 0$ and $\frac{\partial C}{\partial x} = 0$
CL5	$U = 0\,;\, V = 0\,;\, T_w = 1$ and $\frac{\partial C}{\partial y} = 0$
CL6	$U = 0\,;\, V = V_0\,;\, T = T_0$ and $C_w = C_0$

Variables present in the previous Eqs. $(1) - (5)$ are rendered dimensionless using H, U_0, $U_0\,/H$, $\rho_0$and $\rho_0 U_0^2$ as scaling variables for length, velocity, time, density and pressure respectively. Whereas the non dimensional temperature and concentration are defined here as follows:

$$T = \frac{(T^* - T_0^*)}{(T_w^* - T_0^*)} \text{ and } C = \frac{(C^* - C_0^*)}{(C_w^* - C_0^*)}$$

The thermal expansion coefficient, solute expansion coefficient, thermal Grashof number and solute Grashof number are respectively:

$\beta_T = -\frac{1}{\rho}(\partial\rho/\partial T)_C$, $\beta_C = -\frac{1}{\rho}(\partial\rho/\partial C)_T$;

$Gr_T = \frac{g\,\beta_T\,\Delta T\,H^3}{\vartheta^2}$ and $Gr_S = \frac{g\,\beta_C\,\Delta C\,H^3}{\vartheta^2}$

The governing dimensionless parameters appearing in the above equation system are: The Reynolds number $Re = U_0\,H/\vartheta$, the Prandtl number $Pr = \vartheta/\alpha$ and the Schmidt number $Sc = \vartheta/D_{Mass}$. Where, ϑ, α and D_{Mass} indicate respectively, the kinematic viscosity, the thermal and mass diffusivities.

The numerical code solves the primitive fields' equations (velocity, pressure) by a finite-volume method. This well known technique developed by Patankar (1980) is currently the most popular method in computational fluid dynamics. A two-corrector step process is applied for diffusive terms. These choices have been validated for free jet configuration by Knani *et al.* (2001). Then, it was adapted to the thermo-solutal confined wall jet configuration in the present study. For the convection diffusion problem, a Hybrid difference scheme (Patankar and Spalding 1970) is retained in the numerical process as it produces physically realistic solution and has proved to be helpful in the prediction of practical flows. Interested readers shall be referred to (Issa 1986; Spalding 1972; Roache 1976).

Several preliminary runs showed that the dimensionless time interval $t^*U_0/H = 60$ is large enough to visualize vortex emission and shedding mechanism taken place within the jet at a Reynolds number equal to 500 (laminar flow), a Richardson number of 0.01 (forced convection), a Schmidt number fixed at 0.7 and a Prandtl number set equal to $Pr = 7$ (corresponding to water). Accordingly, a series of simulations have been done with diverse time-step values. The obtained results, along with calculation-time consuming considerations, showed that $\Delta t = 0.01$ (namely 6000 images) is a reasonably fair choice owing to the maximum error calculated for average Nusselt number, average Sherwood number and average skin friction coefficient.

The following definitions were employed:

Local quantities:

$$Nu(x) = -\left.\frac{\partial T}{\partial y}\right|_{y=0} \quad (6)$$

$$C_f(x) = \tau_p(x)/\left(\frac{1}{2}\rho U_0^2\right) \quad (7)$$

$$Sh(x) = -\left.\frac{\partial C}{\partial y}\right|_{y=0} \quad (8)$$

Where $\tau_p(x) = \mu\left(\frac{\partial U}{\partial y}\right)_{y=0}$

Mean coefficients values are calculated as:

$$\overline{Nu} = \frac{1}{L}\int_0^L Nu(x)\,dx \quad (9)$$

$$\overline{Sh} = \frac{1}{L}\int_0^L Sh(x)\,dx \quad (10)$$

$$\overline{C_f} = \frac{1}{L}\int_0^L C_f(x)\,dx \quad (11)$$

3. RESULTS AND DISCUSSION

3.1 Code Validation

The base flow is computed using a two-dimensional numerical simulation code (2D-NS). Velocity profiles obtained from the 2D-NS code are compared with theoretical finding established by Glauert (1956) plotted in Fig. 2. A good agreement is achieved. The principal parameters for such flow are: maximum streamwise velocity component U_{max}, wall jet width δ (the point where stream wise velocity profile reaches its maximum) and wall jet half width $\delta_{1/2}$ (the distances from the wall where the velocity reaches its half local maximum in the outer region). The corresponding maximum deviation percentages of numerical results in comparison with theoretical data calculated for each parameter are around 7.4, 4.8 and 6.0, respectively. Thus, since the maximum deviation is smaller than 8% , the present code is adequate to simulate the physics of the studied wall jet flow properly.

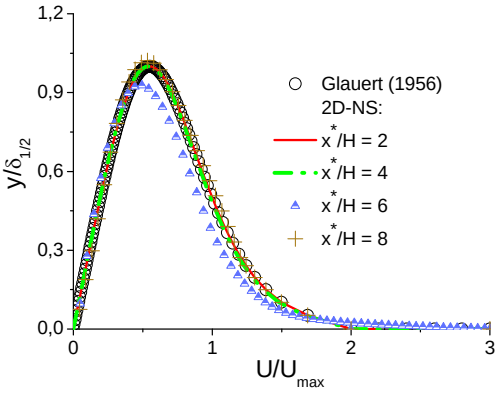

Fig. 2. Comparison between Numerical results and theoretical Glauert (1956) solution.

3.2 Structure of the Uncontrolled Flow

It is worth note that the Reynolds number is fixed to 500 in all next computations. This value was fixed after previous simulations conducted over a range between 100 and 1000. Numerical results indicated that for low Reynolds number, the ratios between the Nusselt and Sherwood coefficients values corresponding to the two considered cases ($v_w = \pm 0.2$) are very small and become larger as far as viscosity decreases. The opposite is true for the skin friction distributions. So, we decide to study an intermediate case where the relative difference between uniform suction and blowing effectiveness is neither so weak nor so strong.

The time-evolving natural dynamics is discussed here, by means of streamlines evolution plotted in Fig. 3. Usually, wall jet interaction with ambient flow is driven primarily by perturbations at the shear layer interface and near the wall. Herein, we can see this flow oscillation that develops naturally in the jet

shear layer, from the first moment, in sections near the entrance approximately at $2 \leq x \leq 3$. In the next time step, this instability grows and rolls-up between the stations $3 \leq x \leq 4$. Typically, such instability called Kelvin-Helmholtz leads to discrete vortex forming. At $t = 15$, we can distinguish a primary vortex emission located around $3.5 \leq x \leq 4.5$. With respect to time, it enlarges and undergoes a shedding phenomenon that begins between $5 \leq x \leq 6$ and ends at $t = 55$ by giving a new finer structure. When $t = 60$, it gradually leaves the studied field and the same phenomenon begins again farther upstream. We may also note the presence of a recirculation cell which size is reduced by the clockwise rotating structure development. As a consequence, this counter-clockwise zone's center is gradually moved toward the domain inlet.

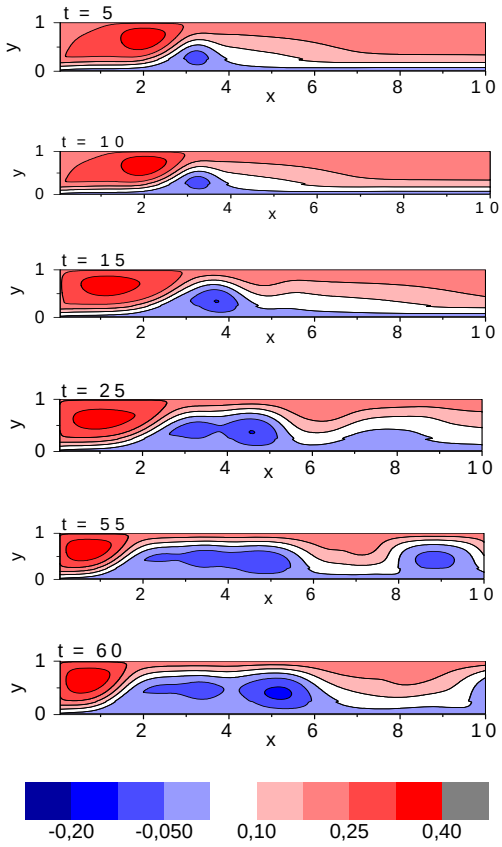

Fig. 3. Streamlines of the natural flow for $Re = 500$.

3.3 Characterization of the Control Technique Effectiveness

3.3.1 Combined effect of Suction or Blowing Slot Length and Lewis Number

The first step of the performance improvement focuses on the combined effect of the slot length and the Lewis number. A particular location of the suction or blowing slot is fixed approximately at $x = 3$. In fact, as we demonstrated in subsection 3.2, this choice represents a critical value from where the natural disturbance starts to roll-up causing a vortex emission little further downstream (between $3.5 \leq x \leq 4.5$.). Moreover, after several computations carried out with respect to the control position, we found that the wall jet flow can be characterized as one of three types for a fixed slot length (no vortex, no shedding and shedding as will be discussed in subsection 3.3.2). The first regime corresponding to an inhibition of the natural vortex emission is associated to a threshold value of $x = 3$. Thus, in this section we prefer to place the slot at this particular position so that the key parameter permitting potential vortices generation and shedding phenomena onset is the control length, l_s, and hence we can determine the corresponding critical values.

Three cases are considered: l_s equal to $2H = 0.5$, $4H = 1$ and $8H = 2$. These values are chosen based on the recirculation cell core scale, l_{RC}, present at the first time step within the natural flow which is around $l_{RC} = 4H$.

Furthermore, it is well known that for double diffusion problems one of the most governing parameters is the Lewis number defined as the ratio between the thermal and mass diffusivity. Bennacer and Gobin (1996) showed that for Lewis number larger than unity, thermal diffusion proceeds at a higher speed than species diffusion as well as thermal boundary layer thickness is greater than solutal boundary layer. This behavior is verified in our study for several numerical combinations considering water flow under aiding buoyancy forces.

Figures 4, 5 and 6 as well as Tables 2 and 3 illustrate the mutual effects of slot length and Lewis numbers when uniform amounts of suction or blowing are imposed. As shown in Fig. 4 and Fig. 5, varying this last parameter does not greatly change the jet dynamics. Consequently, the derived skin friction distribution is rather constant with increasing *Le* over a wide range in all computed cases (see Tables 2 and 3). However, concentration contours (plotted at the bottom in the same figures Fig. 4 and Fig. 5) reveal strong vertical solutal stratification. The observed phenomena intensity

decreases with increasing Lewis number and iso-concentration lines start to curve particularly for blowing. As a result, mass diffusion takes place mainly in the longitudinal direction. This outcome designates a very diffusive flow behavior which yields significant mass transfer amplification as denoted in all simulations. However, heat transfer coefficient distribution plotted in Fig. 6 (a) and (b) is almost constant. One possible explanation is that the strong vertical concentration field stratification restricts temperature diffusion which makes mean Nusselt number evolution almost independent of Lewis number.

Oueslati *et al.* (2013) found that as N increases from 0 to 8 at aiding flow situation $(N > 0)$, species structures become more horizontally stratified. However, thermal contribution seems not to be much modified when compared to isotherms corresponding to the limit flow $(N = 0)$. In the present paper N is kept equal to 10. In case of blowing, all computations carried out under this

aiding water flow situation showed that as the slot length is increased, the concentration contours stratification become more obvious as depicted in Fig. 5. This means that the solutal boundary layer becomes thicker as l_s enlarge which reduces the mass transfer rate in blowing cases (Table 2).

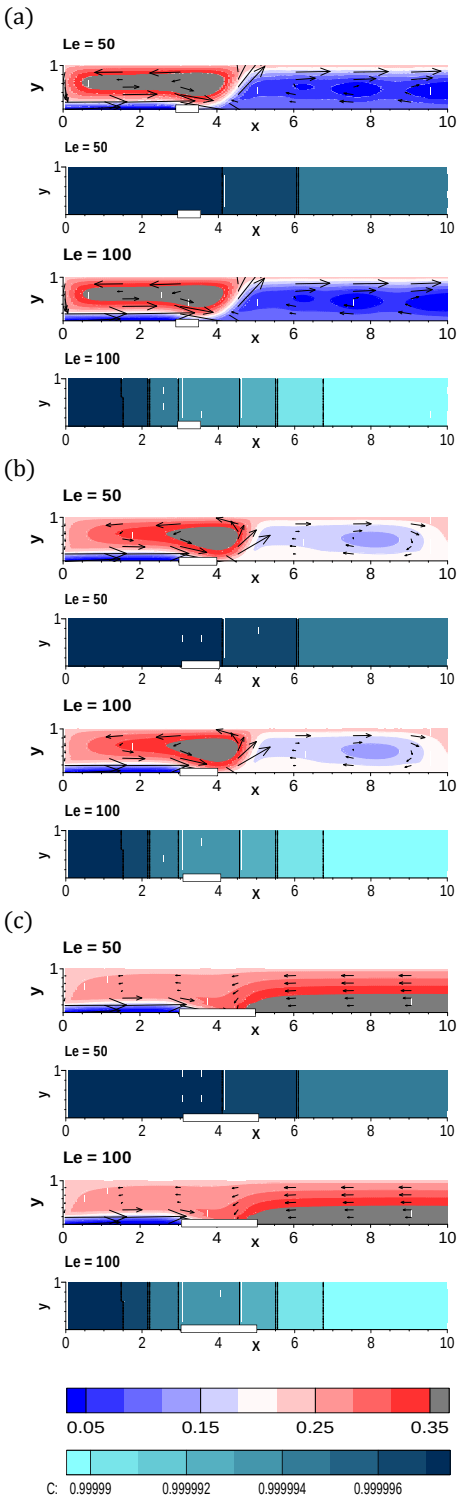

Fig. 4. Streamlines (at top) and iso-contours of concentration (at bottom) corresponding to suction at two Lewis number and $Re = 500$ (a) $l_s = 2H$, (b) $l_s = 4H$, (c) $l_s = 8H$.

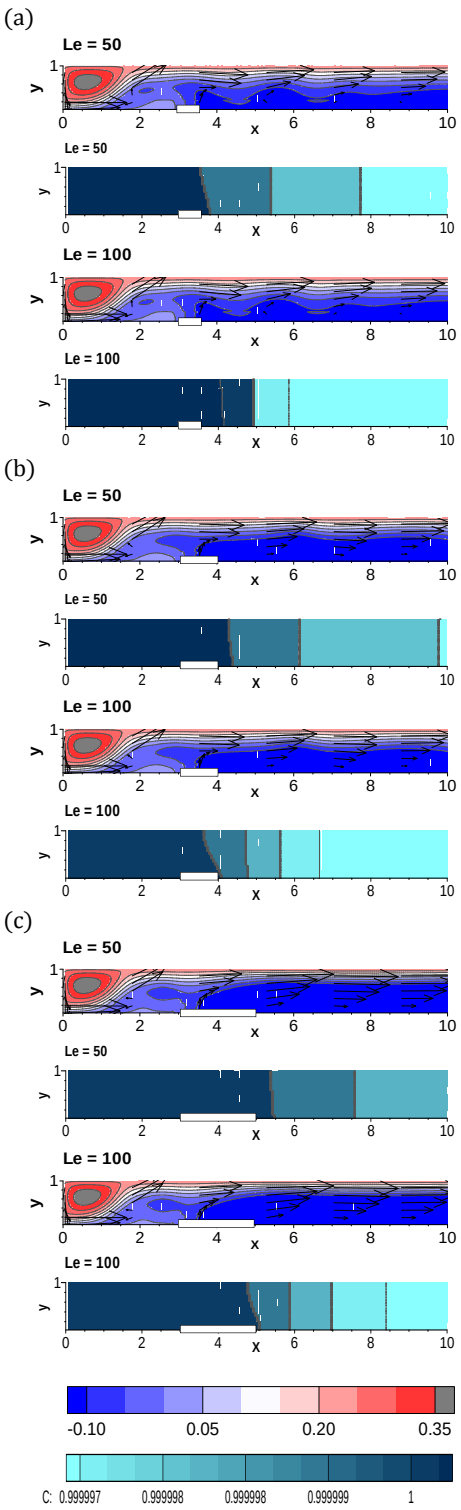

Fig. 5. Streamlines (at top) and iso-contours of concentration (at bottom) corresponding to blowing at two Lewis number and $Re = 500$ for (a) $l_s = 2H$, (b) $l_s = 4H$, (c) $l_s = 8H$.

Moreover, increasing l_s amplify the uniformly introduced water amounts which intensify the jet energy aspect and tends to stabilize outer region perturbation especially downstream of the nozzle. This is indicated by the streamlines plotted in Fig. 5

Table 2 Values of averages coefficients at three blowing slot lengths for $\mathbf{Re = 500}$ skin friction coefficient $(\mathbf{10^{-3}})$, Sherwood number $(\mathbf{10^{-5}})$ and Nusselt number

Le	$\overline{C_f}$			$\overline{Nu}$			$\overline{Sh}$		
	$l_s = 2H$	$l_s = 4H$	$l_s = 8H$	$l_s = 2H$	$l_s = 4H$	$l_s = 8H$	$l_s = 2H$	$l_s = 4H$	$l_s = 8H$
10	4.387702	4.239679	3.943918	1.12878	1.361816	1.626264	2.164578	1.951215	1.635671
20	4.387676	4.239664	3.943908	1.128779	1.361796	1.626263	2.311307	2.106223	1.803315
30	4.387649	4.239649	3.943898	1.128770	1.361775	1.626262	2.460856	2.263845	1.973230
40	4.387622	4.239633	3.943888	1.128761	1.361754	1.626261	2.613188	2.424039	2.145377
50	4.387594	4.239617	3.943878	1.128752	1.361732	1.626259	2.768269	2.586770	2.319721
60	4.387565	4.239600	3.943867	1.128743	1.361710	1.626258	2.926054	2.751993	2.496212
70	4.387538	4.239583	3.943857	1.128733	1.361687	1.626257	3.086498	2.919667	2.674818
80	4.387508	4.239566	3.943846	1.128723	1.361664	1.626255	3.249560	3.089740	2.855486
90	4.387478	4.239548	3.943834	1.128713	1.361640	1.626254	3.415190	3.262169	3.038175
100	4.387447	4.239530	3.943823	1.128703	1.361616	1.626252	3.583335	3.436899	3.222834

that becomes less curved and more intense which promotes heat transfer and therefore enhances the Nusselt number (see Fig. 6 (a)). Seifert *et al.* (1996) confirmed that blowing increases boundary layer momentum. In particular, perpendicular blowing increases flow turbulence as a result of adding energy to the mean flow. Therefore, for advanced blowing amplitude or jet width, more eddies become larger (Yousefi and Saleh 2014).

Regarding wall forces, increasing l_s continues to yield better skin friction reduction. As the slot extends, the fluid is lifted up and accelerates in the outer region. Accordingly, the wall skin friction coefficient becomes weaker (Table 2).

If suction is applied, we found that jet pattern depends strongly in the slot length as illustrated in Fig. 4. While increasing l_s, the controlled flow structure becomes more complicated and exhibits vortex shedding mechanism.

For the smallest nozzle $l_s = 2H$, streamlines reveal two major counter-rotating cells. The counter clockwise one escapes the suction effect and extends approximately to $x = 4.5$. The clockwise vortex develops with respect to time and an initiation of detachment phenomena takes place near the studied domain outlet. When l_s is set equal to $4H$, all structures intensities, which centers are advected downstream, are weakened and vortex shedding is suppressed. Further suction slot expansion $l_s = 8H$, inhibits vortex formation due to earlier evacuation of the recirculation cell through the nozzle. From these results it can be concluded that when the slot length exceeds the recirculation cell size, this latter is removed which suppresses the primary and secondary structures emission.

According to the previous observations, the wall jet characteristics show three states as suction slot length is increased: 'shedding', 'no shedding' and 'no vortex'. A general classification of these phases can be generated as follows:

For $l_s < l_{RC}$, shedding phenomena takes place behind the slot;

For $l_s = l_{RC}$, vortex creation occurs but no shedding processes;

For $l_s > l_{RC}$, vortex emission is suppressed.

Here l_{RC} which denotes the natural recirculation cell length represents the critical value of vortex and shedding onset.

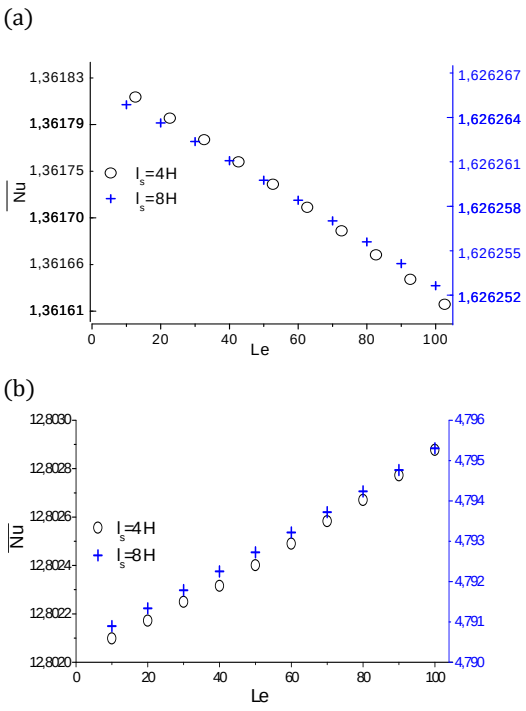

Fig. 6. Average Nusselt number distribution at two slot lengths corresponding to (a) blowing $(v_w = +0.2)$, (b) suction$(v_w = -0.2)$.

Similarly, three flow regimes (no separation, separation, and shedding) were also observed by Chen *et al.* (2006) on laminar boundary layer depending on the blowing rate. They found that the critical values corresponding to separation and

Table 3 Values of averages coefficients at three suction slot lengths for $Re = 500$ skin friction coefficient (10^{-3}), Sherwood number (10^{-6}) and Nusselt number

Le	$\overline{C_f}$			$\overline{Nu}$			$\overline{Sh}$		
	$l_s = 2H$	$l_s = 4H$	$l_s = 8H$	$l_s = 2H$	$l_s = 4H$	$l_s = 8H$	$l_s = 2H$	$l_s = 4H$	$l_s = 8H$
10	8.951726	7.989010	6.140131	14.978817	12.802099	4.790900	1.528789	1.528797	1.528798
20	9.117782	7.988970	6.140108	14.471161	12.802172	4.791338	1.605914	1.605936	1.605938
30	9.117769	7.988929	6.140085	14.471058	12.802249	4.791788	1.684814	1.684849	1.684853
40	9.117756	7.988887	6.140061	14.470954	12.802315	4.792252	1.765472	1.765522	1.765528
50	9.117744	7.988845	6.140037	14.470849	12.802400	4.792728	1.847870	1.847936	1.847945
60	9.117733	7.988802	6.140013	14.470743	12.802490	4.793218	1.931993	1.932077	1.932090
70	9.117723	7.988759	6.139988	14.470637	12.802583	4.793720	2.017819	2.017920	2.017937
80	9.117714	7.988715	6.139963	14.470530	12.802670	4.794235	2.105323	2.105445	2.105468
90	9.117706	7.988670	6.139937	14.470422	12.802772	4.794762	2.194483	2.194627	2.194655
100	9.117699	7.988625	6.139911	14.470314	12.802877	4.795302	2.285273	2.285440	2.285477

shedding decrease with increasing Reynolds Moreover, each state properties are reflected by averages flow coefficients characteristics (see Table 3). Thus, the longest suction slot allows significant skin friction as well as Nusselt number reduction. This confirms once again the crucial role of flow structure in heat exchange.

A more detailed study of the involved parameters effects on skin friction and thermo-solutal quantities can be provided from Tables 2 and 3. The simulated values range between $10 \leq Le \leq 100$.

In case of wall blowing, we found that heat transfer coefficient is almost independent of Le (slightly decreases) at all slot length values. However, Sherwood number increases noticeably (see Table 2). Thus, the studied parameter influence is much more important in mass transfer than in heat transfer. This is logic since the only factor tuned at a constant Prandtl number is the Schmidt value of the fluid. Similar behaviors were found by several works such as Bansod (2005). He investigated blowing and suction effects on double diffusion by mixed convection over inclined permeable surfaces. His results showed that Nusselt number decreases for all tested control parameter, whereas Sherwood number increases with Lewis number for the positive values. Note that the mentioned control parameter is positive for fluid withdrawal, negative for discharging and equal to zero for impermeable vertical flat plate embedded in a porous medium. Also, Zhao *et al.* (2007) studied the free convection from one thermal and solute source in a confined porous medium. They showed that the Lewis number has a direct bearing on heat and mass transfer coefficients. As it was amplified, the Sherwood number consistently increases but the average Nusselt number decreases.

Lewis number effect on laminar thermo-solutal convection in vertical cavities with uniform, constant temperature and mass fraction profiles was recently studied numerically by Sun and Lauriat (2010). Two values were considered $Le = 0.5$ and $Le = 2$ for aiding buoyancy forces at a fixed Prandtl number corresponding to air $Pr = 0.71$. They showed that the mean Nusselt number decreases slightly with Le while Sherwood number enhancement is much more significant. They explain this $\overline{Nu}$ distribution tendency by a weak thermal boundary growth and mainly by the reduction of its advective part due to blowing effect as Le increases. Concerning $\overline{Sh}$ improvement, it is associated with the solutal boundary layer thinning with varying the Lewis number. Similar behaviors are found in the present study.

Suction has the opposite effect on average Nusselt number distribution regarding both studied parameters (Lewis number and the slot length) as shown in Table 3. Indeed, even if $\overline{Nu}$ evolution with Le is almost negligible (of about 10^{-3}), we shall note that it increases slightly for all considered nozzle lengths except for $l_s = 2H$. This behavior may be caused by vortex detachment phenomena observed only in this last case (see Fig. 4). Although, Table 3 shows that average Sherwood number is enhanced by Le as in blowing case but the slot length effect becomes negligible. This aspect is indicated by the quite similar solutal contours obtained for all computed values of l_s at a fixed Lewis number.

Moreover, it is obvious from the two above approaches that the hydrodynamic skin friction distribution depends barely on Lewis number but strongly on the slot length. For blowing, the lowest values of $\overline{C_f}$ and $\overline{Sh}$ are obtained at the largest slit (Table 2). However, the maximum $\overline{Nu}$ reduction corresponds to the narrowest one. In the same way Abdulla and Jassim (2010) found that the widest slot from the three tested values equal to 0.28 m ; 0.2 m and 0.12 m give the maximum skin friction coefficient reduction for uniform blowing. This

combined effect of source length and Lewis number was also simulated numerically by Oueslati *et al.* (2013). The study concerns a double-diffusive natural convection in an enclosure with a partial vertical heat and mass source for an aspect ratio $A = 4$. The authors found that the mean Nusselt number slightly decreases with Lewis number in the range $10 \leq Le \leq 100$ at all source length values $0.25 \leq d \leq 2$. In contrast, the mass transfer rate is greatly enhanced by increasing Le. Moreover, they demonstrated that the highest values of $\overline{Nu}$ and $\overline{Sh}$ are associated with the longest source ($d = 2$). The present work presents similar finding except for the maximum $\overline{Sh}$ which corresponds to the smallest slot (In reality, this last observation is consistent with our configuration in case of wall suction). That's may be due to the two different boundary conditions since here the concerned slot is not a discrete concentration source as in their work.

If suction is applied (see Table 3), we found that mean skin friction coefficient dependency on Le is negligible at all slot lengths. Moreover, we note that the widest slot from the three tested values give the highest $\overline{C_f}$ and $\overline{Nu}$ reductions. It is worth noting that varying l_s from $2H$ to $4H$ then $8H$ decrease heat transfers by 11.5 % and 62.5 %, respectively. This significant drop observed in the last case ($l_s > l_{RC}$) is linked to vortex and shedding suppression. However, the highest $\overline{Sh}$ value corresponds to the longest one. In fact, mass coefficient evolution dependency in wall suction slot size appears to be negligible.

A comparison between the two methods under the same flow conditions shows that blowing is more effective than suction in skin friction coefficient as well as thermal transfer reduction. Moreover, the quite large difference efficiency of these two control approaches regarding Sherwood number distributions depending in the slot length are due to initial boundary conditions. As we mentioned previously, the concentrated water is injected from the jet entry for suction and from the horizontal slot for blowing. Thus, the slot length effects are more obvious in the last case.

In conclusion, increasing Lewis number enhances mass transfer coefficient in all simulations. The explanation is that since the convection term rises relatively to the diffusion term in the species conservation Eq. (5), the solutal boundary layer becomes thinner and so $\overline{Sh}$ increases. For suction the maximum fluid force reduction is obtained in the optimum condition where the vortex shedding weakens or even suppresses as the slot length enlarges. In case of blowing, wider slot gives better control effectiveness in skin friction reduction terms. The same results were found by Yukinori *et al.* (2015) indicating that as the controlled region becomes wider in the stream-wise direction, the control effect on the skin friction drag becomes larger for both blowing and suction cases.

3.3.2 Suction or Blowing Slot Position

Summarizing the above results, the vertical wall suction or blowing applied at natural vortex emission location cannot suppress shedding phenomena behind the slot unless the length of this later is larger than a threshold value. Even so, we still have relatively high skin friction coefficient.

In this section, the proposed method is to move the slot location over the entire domain by step of unity in order to inhibit the onset of the instability itself in earlier stages. In all next simulations, the nozzle length is set equal to unity ($l_s = 4H = 1$).

Figure 7 depicts controlled flow patterns when blowing is applied. For $x_s = 1$, natural shear layer instability mode is removed. Water flow emanating from the horizontal nozzle rises up the jet and slowly occupies all the remaining space. Around $t = 45$, a steady state is established and the flow structure becomes well defined. For $x_s = 2$ and $x_s = 3$, no great changes are noted except that the recirculation cells are quite larger and the steady state is further delayed as the inner region oscillation becomes more pronounced.

Starting from $x_s = 4$ since the blowing nozzle is located deep in the natural vortex emission region or beyond, the main flow structure is significantly altered. Upstream of the slot, Kelvin-Helmholtz instability develops relatively similar to the natural case. However, the emission of the primary vortex, which is now smaller and is rejected towards the entrance, is delayed to $t = 15$. At the next moment $t = 20$, it joins the introduced water movement and vanishes within it due to advection forces. This cycle is repeatedly observed for the remaining computed time. For $x_s = 5$, same steps are observed (vortex creation then combination with the introduced flow) but over wider intervals. The explanation is simple since the slot is located further the structure takes more time to reach it at $t = 35$.

From $x_s = 6$, a vortex shedding mechanism takes place as in the natural case but it begins upstream and ends earlier around $t = 45$. This new structure is directly intercepted by the added flow. Whereas, the primary vortex continues to grow until it also reaches the mean motion by the last time step.

Qualitatively, the same observations apply equally to the last two stations $x_s = 7$ and $x_s = 8$. However, simulated time is not enough anymore for the swirl to join these positions. Thus, more structures are present at the same time steps compared to $x_s = 6$.

When suction is applied, the first three conditions give almost similar patterns as represented in Fig. 8. Streamlines corresponding to the two first cases $x_s \leq 2$ show that the recirculation cell escapes the control influence and it is convected to the upper edge of the nozzle. A small structure emergence at $t = 15$ and $t = 20$ is also denoted corresponding to $x_s \leq 2$ and $x_s = 3$, respectively. It becomes larger and intensifies as the simulation time runs.

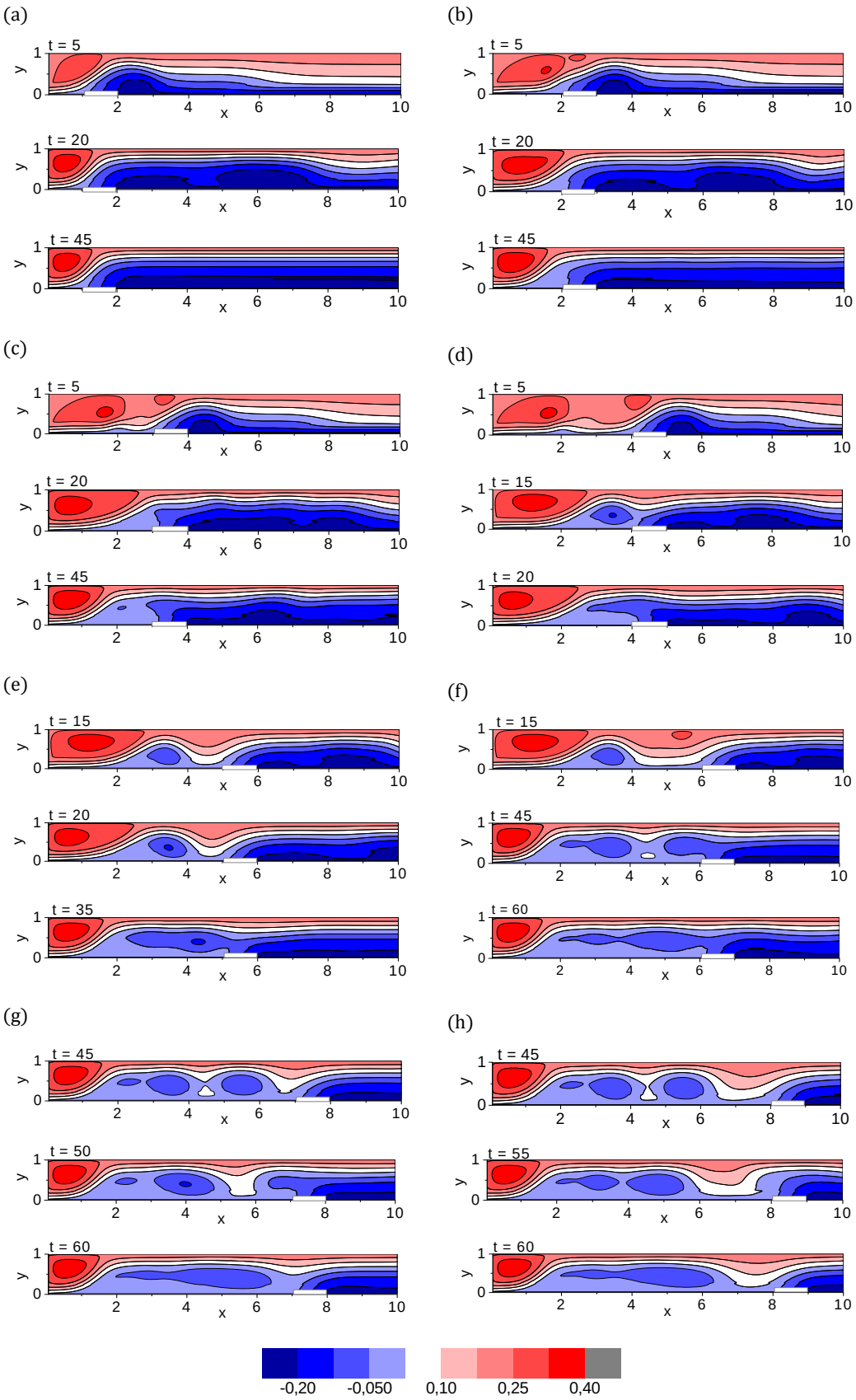

Fig. 7. Streamlines evolutions corresponding to blowing at (a) $x_s = 1$, (b) $x_s = 2$, (c) $x_s = 3$, (d) $x_s = 4$, (e) $x_s = 5$, (f) $x_s = 6$, (g) $x_s = 7$, (h) $x_s = 8$.

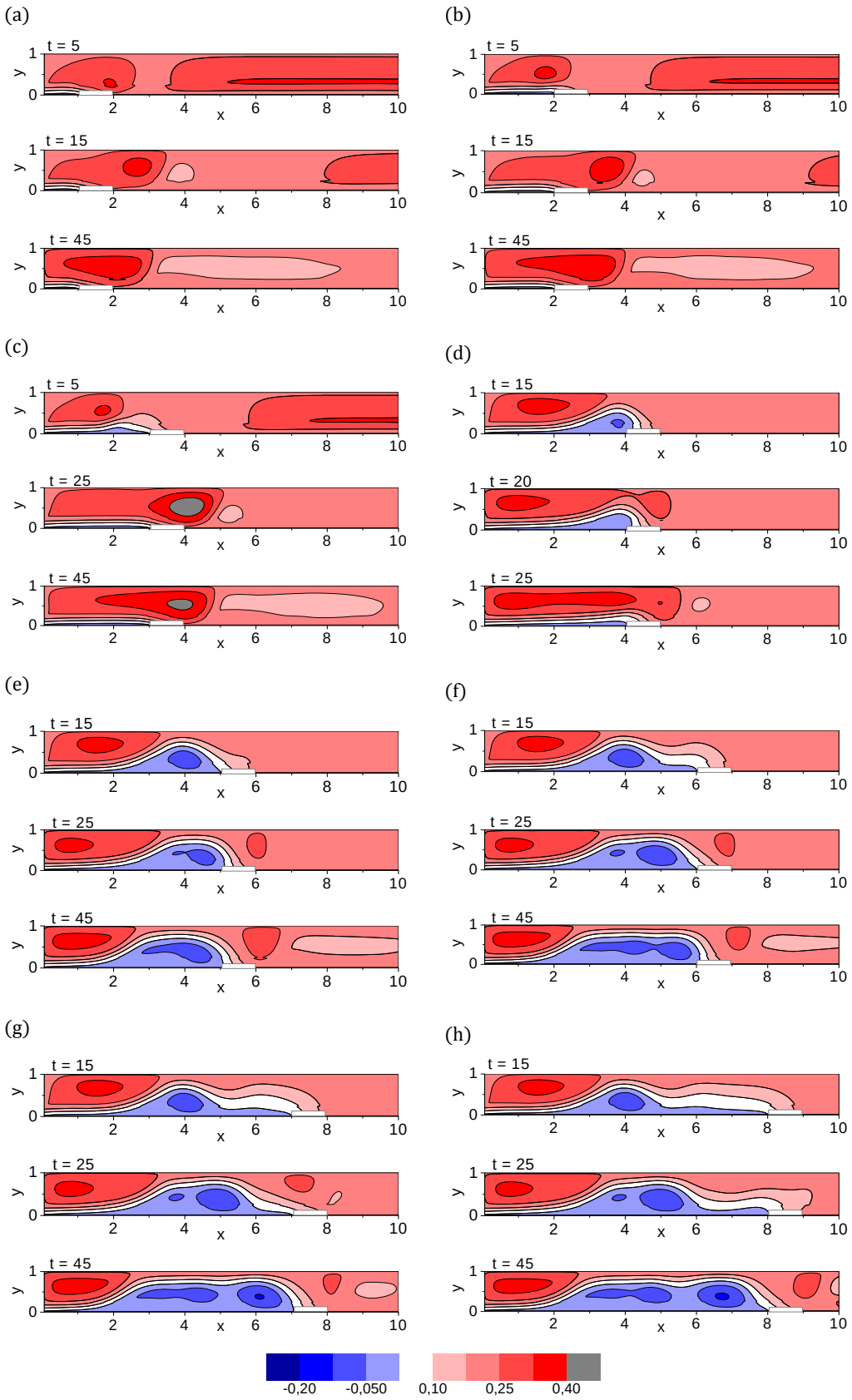

Fig. 8. Streamlines evolutions corresponding to suction at (a) $x_s = 1$, (b) $x_s = 2$, (c) $x_s = 3$, (d) $x_s = 4$, (e) $x_s = 5$, (f) $x_s = 6$, (g) $x_s = 7$, (h) $x_s = 8$.

Note that in the third case $x_s = 3$, the negative vorticity becomes wider and the creation of the positive one is delayed compared to both last cases ($t = 20$).

Starting from $x_s = 4$, the upstream flow dynamic is similar to that observed in the uncontrolled jet since the nozzle is roughly located beyond the natural vortex emission position. However, at the same time step, $t = 15$, this latter is less developed then it is evacuated through the slot at $t = 20$. At the next moment, the ordinary spatial organization governed by the two counter-rotating cells begins from $t = 25$ which is slightly later than previous simulations. For $x_s = 5$, the primary vortex follows the same growth as in natural flow until $t = 15$. However, instead of being aspirated with the main flow, it adheres to the lower edge of the slot $x = 4$. Moreover, the downward fluid motions at the vortex extremity along with the wall friction forces yield a new counter-rotating region (i.e. turning in the same direction as the recirculation zone). This zone is located at the upper edge of the slot $x = 5$. At the same time step $t = 25$, another clockwise rotating structure appears due to interactions between this new negative vorticity cell and the water sucked in the opposite streamwise direction. As computational time turn, about $t = 45$ we note that being stopped at the slot edge, the primary vortex development simultaneously moves the two recirculation zones which surround it. Approaching simulation time's end, these two regions diminish being confined by the vertical plate at the inlet and by the base flow at the exit, respectively. For the remaining cases $x_s \geq 6$, the derived streamlines almost exhibit similar behavior and an initiation of shedding phenomenon takes place which becomes even more obvious for $x_s = 8$.

From previous simulations, critical slot position values can be arranged as follows:

For $x_s < 3$, no natural vortex emission;

For $4 \leq x_s \leq 5$, no shedding,

For $6 \leq x_s$, shedding.

Note that these critical values are directly related to the natural vortex and shedding onset locations.

This arrangement can be clearly recognized from averages flow characteristic coefficient distributions plotted in Fig. 9. It is shown that the studied domain can be decomposed into two parts according to the natural vortex generation position. Here, it is located in vicinity of $3.5 \leq x \leq 4.5$, as mentioned in subsection 3.2. This decomposition is indicated by an inflection in the skin friction, mass and heat coefficient profiles. Locating the slot in the next station $x_s = 5$ shows particular jet response for both suction and blowing. It gives thresholds values of the different settings.

In case of blowing approximately for $x_s \leq 4$, we see that $\overline{C_f}$, $\overline{Nu}$ and $\overline{Sh}$ slightly increase with x_s. For downstream stations $x_s \geq 4$, thermo-solutal coefficient distributions monotony change and their values decrease rapidly approaching the exit. Moreover, the maximum skin friction coefficient reduction is observed at $x_s = 6$. Wall suction yields opposite behaviors except for $\overline{C_f}$ which distribution shows even a better remarkable separation between the two parties. Moreover, we found that this control approach has less effect on hydrodynamic force reduction when it is located in front of the natural vortex position. Note that suction generates stronger skin friction coefficient and larger double diffusion rates than blowing. Moving slot location toward the domain outlet (behind natural vortex creation) reduces the relative effectiveness of suction over blowing very substantially regarding skin friction distribution. The difference is attributed to the control position relative to the natural vortex emission point that is now upstream of the slot.

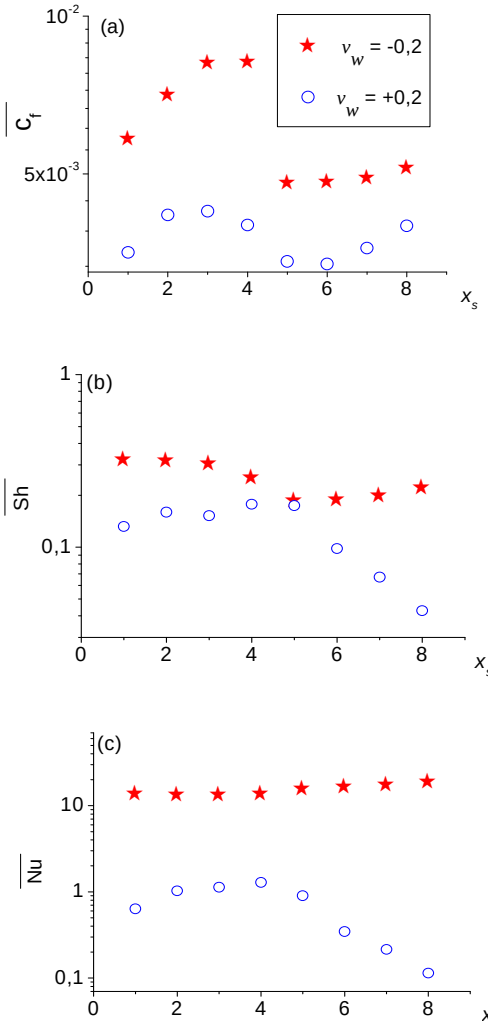

Fig. 9. Averages (a) skin friction, (b) Sherwood number and (c) Nusselt number evolutions corresponding to $v_w = -0.2$ and $v_w = +0.2$ for $Re = 500$.

Earlier study of Bansod (2005) showed that heat and mass transfer increase with suction and decrease with blowing. Herein we also found that $\overline{Nu}$, $\overline{C_f}$ and $\overline{Sh}$ are increased by suction compared to blowing.

Considering the control location, Chen *et al.* (2015) suggested that suction has less effect on aerodynamic force coefficients when the control holes are located in front of the separation point or deep in the flow separation region. However, the best effectiveness is reached when the azimuthal suction holes location is very close to the separation point. A comparison with Trompoukis *et al.* (2008) may seem right. The authors showed that with fixed slot position, any increase in the suction rate leads to reduction in the flow separation length. Moreover, locating the slot over the ramp, just downstream of the separation onset, yields better performance. In the present paper, the best skin friction reduction in case of suction is granted by widening the slot and locating it just downstream of the natural vortex generation position.

4. CONCLUSION

In this study, thermo-solutal transfers and fluid dynamics of a two-dimensional confined wall jet have been simulated numerically. The laminar flow is subjected to high level uniform amounts of suction or blowing from a thin opening implanted on the bottom heated wall. It has been found that the slot geometrical characteristics as well as the Lewis number are ones of the most crucial parameters governing such active flow control technique. Some critical values were obtained beyond which vortices are formed and shed alternately behind the slot. It was demonstrated that these values depend on the natural instability onset. The second purpose was to evaluate each flow state on double diffusion rates. It was concluded that hydrodynamic flow force and mass and heat exchanges can be enhanced or reduced following the inhibition or improvement of clockwise and counter clockwise vortical structure.

Moreover, it was proved that as Lewis number increases, average Nusselt number is almost constant but average Sherwood number is noticeably improved. Furthermore, it was shown that maximum heat transfer enhancement corresponds to the largest slot. However, maximum mass transfer is granted by the smallest one. This last effect becomes negligible when suction is imposed. Numerical results also showed that the control slot position can play a significant role on flow patterns. We found that the studied domain can be decomposed into two sub-domains according to natural vortex emission location.

In conclusion, when suction is applied, widening the slot and locating it upstream of natural vortex emission position can suppress its formation. When blowing is imposed, further increase of these parameters continues to achieve larger skin friction reduction.

ACKNOWLEDGEMENTS

The Authors would like to acknowledge Mr. Henri Claude Boisson Research Director at CNRS of the Fluid Mechanic Institute Toulouse, Professors Christophe Airiau and Pierre Brancher of University Paul Sabatier Toulouse for numerical code development and their helpful comments.

REFERENCES

Abdulla, N. N. and S. L. G. Jassim (2010). Parametric study of suction or blowing effects on turbulent flow over a flat plate. *Journal of Engineering* 16(4), 6164-6185.

Bansod, V. J. (2005). The effects of blowing and suction on double diffusion by mixed convection over inclined permeable surfaces. *Transport in Porous Media* 60(3), 301-317.

Bennacer, R. and D. Gobin (1996). Cooperating thermosolutal convection in enclosures: Scale analysis and mass transfer. *International Journal of Heat and Mass Transfer* 39(13), 2671-2681.

Chen, C., R. Seele, and I. J. Wygnanski (2010). On the Comparative Effectiveness of Steady Blowing and Suction Used for Separation and Circulation Control on an Elliptical Airfoil. *40th AIAA Fluid Dynamics Conference*, Chicago, Illinois, USA, AIAA 2010–4715.

Chen, W. L., Y. Cao, H. Li and H. Hu (2015). Numerical investigation of steady suction control of flow around a circular cylinder. *Journal of Fluids and Structures* 59(11), 22-36.

Chen, X. J., K. Kim and H. J. Sung (2006). Effects of local blowing from a slot on a laminar boundary layer. *Fluid Dynamics Research* 38(8), 539-549.

Glauert, M. B. (1956). The Wall Jet. *J. Fluid Mech.* 1, 625–643.

Issa, R. I. (1986). Solution of the implicitly discretised fluid flow equations by operator splitting. *Journal of Computational Physics* 62(1), 40-65.

Kim, K. and H. J. Sung (2003). Effects of periodic blowing from spanwise slot on a turbulent boundary layer, *AIAA Journal* 41(10), 1916-1924.

Knani, M. A., T. Lili and H. C. Boisson (2001). Response of plane viscous jet to entrance flow rate perturbation. *International Journal for Numerical Methods in Fluids* 37(3), 361-374.

Marom, L., N. Shay and A. Seifert (2016). Stereo PIV measurements of Suction and Pulsed Blowing Interaction with a Laminar Boundary Layer. *18th International Symposium on the Application of Laser and Imaging Techniques to Fluid Mechanics*, Lisbon, Portugal.

Marom, L., V. Palei and A. Seifert (2015). Suction and Pulsed Blowing Interaction with a Laminar Boundary Layer. *55th ISR Aero Conf*.

Oueslati, F., B. Ben Baya, and L. Taieb (2013). Numerical investigation of thermo-solutal natural convection in a rectangular enclosure of an aspect ratio four with heat and solute

sources. *Heat and Mass Transfer* 50(5), 721-736.

Patankar, S. V. (1980). Numerical heat transfer and fluid flow. *Hemisphere Publishing Corporation*, New York.

Patankar, S. V. and D. B. Spalding (1970). Heat and Mass Transfer in Boundary Layers: A General Calculation Procedure. *Second edition, Intertext Books*, London.

Radespiel, R., M. Burnazzi, M. Casper and P. Scholz (2016). Active flow control for high lift with steady blowing. *The Aeronautical Journal* 120(1223), 171-200.

Roache, P. J. (1976). Computational Fluid Dynamics. *Hermosa*, Albuquerque, NM.

Sattarzadeh, S. S and J. H. M. Fransson (2017). Spanwise boundary layer modulations using finite discrete suction for transition delay. *Exp Fluids* 58(14), 1-14.

Seifert, A. and L. Marom (2015). Interaction of suction and pulsed blowing with a laminar boundary layer. *68th Annual Meeting of the APS Division of Fluid Dynamics* 60(21), Boston, Massachusetts.

Seifert, A., A. Darabi and I. Wygnansky (1996). Delay of airfoil stall by periodic extinction. *Journal of Aircraft* 33, 691-698.

Sohankar, A., M. Khodadadi and E. Rangraz (2015). Control of fluid flow and heat transfer around a square cylinder by uniform suction and blowing at low Reynolds numbers. *Comput Fluids* 109, 155–167.

Spalding, D. B. (1972). A Novel Finite difference Formulation for Differential Expression Involving Both First and Second Derivatives. *International Journal for Numerical Methods in Engineering* 4, 551-559

Sun, H. and G. Lauriat (2010). A numerical study based on a weekly compressible formulation for thermo-solutal convection in vertical cavities. *Heat Mass Transfer* 46(5), 495-508.

Sun, M. and H. Hamdani (2001). Separation Control by Alternating Tangential Blowing/Suction at Multiple Slots. *AIAA Journal* 39(4), 735-737.

Trompoukis, X., V. G. Asouti, T. Zervogiannis and K. C. Giannakoglou (2008). CFD Analysis and parametric study optimization of suction-blowing flow control techniques. *6th GRACM International Congress on Computational Mechanics*, Thessaloniki.

Wilson, J., D. Schatzman, E. Arad, A. Seifert and T. Shtende (2013). Suction and Pulsed-Blowing Flow Control Applied to an Axisymmetric Body. *AIAA Journal* 51(10), 2432-2446.

Yousefi, K. and R. Saleh (2014). The effects of trailing edge blowing on aerodynamic characteristics of the Naca 0012 airfoil and optimization of the blowing slot geometry. *Journal of Theoretical and Applied Mechanics* 52(1), 165-179.

Yousefi, K., S. R. Saleh and P. Zahedi (2013). Numerical Study of Flow Separation Control by Tangential and Perpendicular Blowing on the NACA 0012 Airfoil. *International Journal of Engineering* 7(1), 10-24.

Yukinori, K., F. Koji, O. Ramis and S. Philipp (2015). Effect of uniform blowing/suction in a turbulent boundary layer at moderate Reynolds number. *International Journal of Heat and Fluid Flow* 55, 132-142.

Zhang, W., Y. Jiang, L. Li and G. Chen (2016). Effects of wall suction/blowing on two-dimensional flow past a confined square cylinder. *SpringerPlus* 5(985), 1-9.

Zhao, D. J., Y. K. Wang, W. W. Cao and P. Zhou (2015). Optimization of Suction Control on an Airfoil Using multi-island Genetic Algorithm. *Procedia Engineering* 99, 696–702.

Zhao, F. Y., D. Liu and G. F. Tang (2007). Free convection from one thermal and solute source in a confined porous medium. *Transp Porous Med* 70, 407-425.